Multiplexed entangled photon-pair sources for all-fiber quantum networks

Yin-Hai Li,[1] Zhi-Yuan Zhou,[2,3] Zhao-Huai Xu,[1] Li-Xin Xu,[1,*] Bao-Sen Shi,[2,3,†] and Guang-Can Guo[2,3]
[1]*Department of Optics and Optical Engineering, University of Science and Technology of China, Hefei, Anhui 230026, China*
[2]*Key Laboratory of Quantum Information, University of Science and Technology of China, Hefei, Anhui 230026, China*
[3]*Synergetic Innovation Center of Quantum Information & Quantum Physics, University of Science and Technology of China, Hefei, Anhui 230026, China*
(Received 12 June 2016; published 12 October 2016)

The ultimate goal of quantum information science is to build a global quantum network, which enables quantum resources to be distributed and shared between remote parties. Such a quantum network can be realized using only fiber elements, thus deriving the advantages of low transmission loss, low cost, scalability, and integrability through mature fiber communication techniques such as dense wavelength division multiplexing. Hence high-quality entangled-photon sources based on fibers are in high demand. Here we report multiplexed polarization- and time-bin-entangled photon-pair sources based on the dispersion-shifted fiber operating at room temperature. The associated high quality of entanglement is characterized using interference, Bell's inequality, and quantum state tomography. The simultaneous presence of both types of entanglement in multichannel pairs of a 100-GHz dense wavelength division multiplexing device indicates a great capacity in distributing entangled photons over multiple users. Our design provides a versatile platform and takes a big step toward constructing an all-fiber quantum network.

DOI: 10.1103/PhysRevA.94.043810

I. INTRODUCTION

Entanglement is one of the key resources in quantum information processing, which enables a variety of applications such as quantum teleportation [1–3], dense coding [4], and enhanced sensitivity in image and metrology [5–7]. Usually, entanglement can be created in various physical systems based on second- or third-order nonlinear processes. Some instances of entanglement generation include spontaneous parametric down-conversion (SPDC) based on bulk and waveguide nonlinear crystals [8–10], spontaneous Raman scattering and spontaneous four-wave mixing (SFWM) in atomic ensembles [11,12], dispersion-shifted fibers (DSFs) [13–16], silicon waveguides [17–19], and photonic crystal fibers [20]. Through conservation of energy, linear momentum, and angular momentum in these nonlinear interaction processes, entanglement can be created in different degrees of freedom of the photon. The commonly generated forms of photonic entanglement are polarization, time bin, path, and orbital angular momentum [21].

Although various systems can be used for preparing different states of entanglement, for the purpose of constructing a global quantum network and distributing entanglement over remote parties, the generation of photon entanglement within the low-loss transmission window of a fiber is indispensable [22]. Building sources using commercially available DSFs offers evident advantages over other devices for their direct connectivity with fibers, absence of free-space alignment, abundance of cheap readily available fiber elements, and ease of integration for scaling. Also, several mature fiber communication techniques such as dense wavelength division multiplexing (DWDM) and time division multiplexing can be used to enhance information transmission capacity. By using the DWDM technique, the full bandwidth of the fiber can be used, greatly enhancing the transmission capacity of a single fiber channel. For polarization entanglement based on quasi-phase-matching second-order nonlinear waveguides or bulk crystals, active switching and entanglement distribution in DWDM have been realized [23–28]. A recent work also reported multiuser quantum key distributions based on DWDM technique by using polarization-entangled photon pairs generated from a AlGaAs phonics chip [29].

In past decades, advances have been made in preparing polarization- and time-bin-entangled photon sources using DSFs [13–16] and photonic crystal fibers [20]. Also, progress has been achieved in suppressing the intense noise from Raman scattering of photon pairs generated in a DSF using pulse pumping, polarization filtering, time filtering with high-performance superconducting-nanowire single-photon detectors, and cooling with liquid gases [30,31]. The coincidence to accidental coincidence ratio increases to a very high level, enabling quantum information processing tasks to be performed. Very recently, quantum storage of telecom band photonic polarization qubits, time-bin-entangled states, and frequency multiplexed modes in erbium-doped optical fiber have been demonstrated [32–34], showing the potential for implementing long-distance all-fiber quantum networks. All-fiber entangled photon sources are good candidates for achieving this goal. While there are many reports on preparing entangled photon sources based on DSFs, none report on a wavelength multiplexed entangled source based on a DSF, having a similar figure of merits as reported in Ref. [19]. These merits include the realization of entanglement over multifrequency modes, which enable the engineering of complex quantum states, and the compatibility with contemporary telecom fibers and quantum memories as well as chip-scale semiconductor technologies featuring compactness, low cost, and scalability.

*xulixin@ustc.edu.cn
†drshi@ustc.edu.cn

In this work we demonstrate multiplexed entanglement photon sources over three pairs of 100-GHz DWDM channels for both polarization and time-bin based on DSF. Operating at room temperature, our sources have good entanglement quality with a coincidence to accidental coincidence ratio (CAR) of 30 without cooling the DSF with liquid gases. The visibilities are nearly 90% without subtracting background coincidences and reach nearly unity after subtraction. The Clauser-Horne-Shimony-Holt (CHSH) inequality measured for the polarization-entangled source has an S value of 2.38 ± 0.12 with a violation of more than three standard deviations. By quantum state tomography for the time-bin-entangled source, we obtain a fidelity of 0.9120 ± 0.0120 (0.9723 ± 0.0070) without (with) background subtraction. All three channel pairs have high two-photon interference visibilities, indicating that entanglement over multiple users can be achieved. The present multiplexed entangled photon sources are important in realizing an all-fiber quantum network and enhance the transmission capacity using the state-of-the-art DWDM technique.

II. MULTIPLEXED POLARIZATION-ENTANGLED SOURCE

We first characterize the multiplexed polarization-entangled source. The experimental setup [Fig. 1(a)] for generating the polarization-entangled photon source includes a homemade mode-locked fiber laser centered at 1550.1 nm, with a repetition rate of 27.9 MHz and pulse width of 25 ps, for use as a pump beam. The beam is first passed through a variable attenuator to adjust the pump power and then the broadband background fluorescence signal is filtered out using a cascade of 100-GHz DWDM filters. The cleaned pump beam is used to pump a fiber loop incorporating a 300-m DSF for generating polarization-entangled photon pairs by SFWM. The strong pump beam is removed by a cascade of 200-GHz DWDM filters and then a 32-channel 100-GHz DWDM is used for distributing the polarization entanglement of correlated channel pairs (actually, six channels are used in the experiments). The output ports of each channel pair are connected to avalanche photon detectors (APDs) (APD1 and APD2, ID220, ID Quantique, Carouge, Switzerland, free running detection, 20% detection efficiency, 10-μs dead time). The output signals from ADP1 and ADP2 are sent to our coincidence count device (TimeHarp 260, PicoQuanta, Berlin, Germany) (0.4-ns coincidence window). The principle for this fiber loop [Fig. 1(a)] is similar to a Sagnac interferometer loop for generating a polarization-entangled photon source based on second-order nonlinear crystals in the SPDC processes [9].

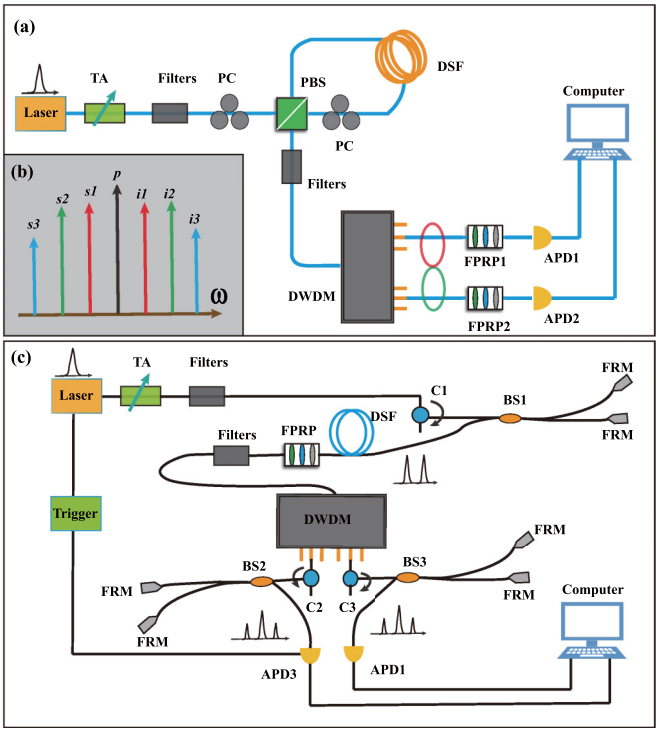

FIG. 1. Experimental setup for multiplexed polarization and time-bin-entangled photon pairs. (a) Setup for polarization-entanglement source. (b) Frequency distribution of pump beam, signals, and idler photon. (c) Setup for time-bin-entanglement source: TA, tunable attenuator; PC, polarization controller; PBS, polarized beam splitter; DSF, dispersion shifted fiber; APD, avalanche photon detector; BS, 2×2 beam splitter; FRM, Faraday rotation mirror; and DWDM, 100-GHz dense wave division multiplexing system.

In the present case, the pump beam is split by a polarized beam splitter (PBS) into clockwise and counterclockwise circularly polarized photon pairs with polarization states $|H\rangle_s|H\rangle_i$ and $|V\rangle_s|V\rangle_i$. After the photon pairs from the two counterpropagation directions recombined at the PBS, the photonic state at the output port of the fiber loop can be expressed as [14]

$$|\Phi\rangle = |HH\rangle + \eta e^{i\delta}|VV\rangle, \tag{1}$$

where η is determined by the ratio of the pump power and $\delta = 2(\varphi_p + \Delta k_p L)$ depends on the initial phase φ_p of the pump beam at the input port and the birefringence $\Delta k_p = k_{pH} - k_{pV}$ experienced by the pump beam in the H and V polarizations. By changing the pump power and initial phase, we can generate maximally entangled states $|\Phi\rangle^{\pm} = 1/\sqrt{2}(|HH\rangle \pm |VV\rangle)$.

To characterize the quality of our entangled source, different methods are used in our experiment. We first measure the two-photon polarization interference fringes under different settings. From the experimental results [Fig. 2(a)], the raw (net) visibilities in the 0° (dashed red line) and 45° (solid black line) bases for channels C31–C37 are $89.33 \pm 1.91\%$ ($96.61 \pm 1.06\%$) and $87.92 \pm 1.95\%$ ($94.39 \pm 1.33\%$), respectively. Visibilities above 71% imply the presence of quantum entanglement.

To further characterize the performance of the entangled source, we measure the S parameter of the CHSH inequality [35], which for the two sets of polarization direction settings ($\theta_s = -22.5°, 67.5°, 22.5°$, and $112.5°$ and $\theta_i = -45°, 45°, 0°$, and $90°$) is 2.38 ± 0.12 without the background subtracted, violating the inequality at more than three standard deviations. After subtracting the background, the S parameter is 2.50 ± 0.12.

To demonstrate the capability of the entanglement distribution over multiple users using wavelength multiplexing, we measure the CARs over three correlated channel pairs by varying the pump power. Because of energy conservation in SFWM, the equal separation of the signal and idler photon frequencies from the pump frequency is correlated; Fig. 1(b)

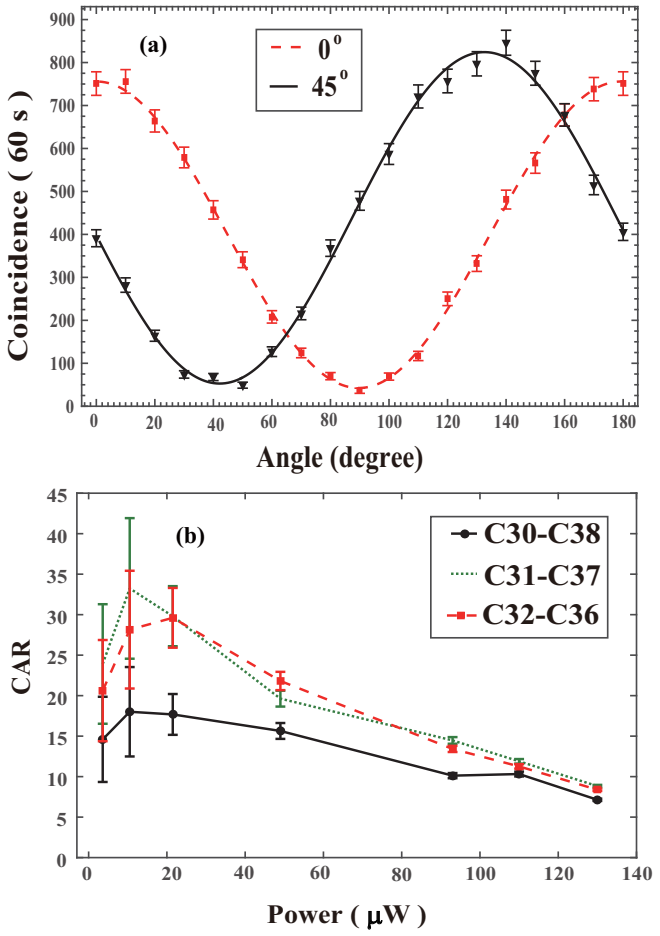

FIG. 2. Two-photon interference fringes and CARs for multiplexed polarization entangled source. (a) Coincidences in 60 s for channel pair C31-C37 as a function of the signal polarizer angle, when the idler angle is fixed at 0° (dashed red line) and 45° (solid black line). (b) CARs for different correlated channel pairs C30-C38 (solid black line), C31-C37 (dotted green line), and C32-C36 (dashed red line) as a function of average pump power.

is a diagram to show this correlation. At the average pump power of 20 μW, the result [Fig. 2(b)] gives a maximum CAR of 30. Channel pairs C31-C37 (dotted green line) and C32-C36 (dashed red line) show similar trends, but channel pair C30-C38 (solid black line) has a relatively lower CAR because the photon spectra in channels C30 and C38 are near the boundary of the emitted photon pairs. The high CAR at room temperature demonstrates that polarization-entangled distribution over multiple users using the DWDM technique is possible. The number of the total correlated channel pairs is limited by the bandwidth of the emitted photon pairs, the measured bandwidth of our present source is around 3.2 nm, and the total correlated channel pairs is at most four pairs.

To know the actual performance of our multichannel polarization-entangled photon pairs, we also measure the visibilities in the 0° and 45° bases for the three channel pairs at an average pump power of 100 μW. The results, listed in Table I, show that all the raw visibilities are greater than 80% and the net visibilities are greater than 96%. The simultaneous presence of high visibilities implies the high quality of our multichannel polarized-entangled photon source. The average losses excluding the detector efficiency for signal and idler photons is around 8 dB. Therefore, the photon-pair generation rate in the 100-GHz bandwidth of the channel pair C3-C37 is 1 MHz, which is equal to 0.11 Hz per pulse.

III. MULTIPLEXED TIME-BIN-ENTANGLED SOURCE

Next we characterize the multiplexed time-bin-entangled source. The time-bin-entangled photon-pair source is another important quantum resource suitable for performing the quantum key distribution over telecom fibers. As in previous experiments, the scheme for time-bin-entanglement generation [Fig. 1(c)] involves using the pump laser and forward and backward filters. The pump beam is split into two time bins by using a 1.6-ns unbalanced Michelson fiber interferometer (UMI) [36,37] consisting of a fiber coupler and two Faraday rotator mirrors. Each pump time bin generates a pair of photons. After removing the pump beam, the generated photon pairs are separated by a 32-channel 100-GHz DWDM. The correlated channel pairs are connected to two UMIs with the same parameters as the first UMI. Each UMI is individually sealed in a copper box and thermally insulated from the air. The temperature of each copper box is controlled with a homemade semiconductor Peltier temperature controller with temperature fluctuations of ± 2 mK. The output of one of the interferometers is connected to APD3 (Princeton Lightwave Inc., Cranbury, NJ, USA, 100-MHz trigger rate, 1-ns detection window, 15% detection efficiency), which is gated by the synchronized signal from the mode-locked laser. The output from the other interferometer is connected to APD1. The electrical detection output signals from APD1 and APD3 are sent for coincidence measurements.

Now we give a brief theoretical description of our time-bin-entanglement source. After the pump beam is divided into two time slots by the forward UMI, the pump photon

TABLE I. Visibilities for different channel pairs for a 100-μW pump and 30-s coincidences.

Channel pairs	Raw V0 (%)	Net V0 (%)	Raw V45 (%)	Net V45 (%)
C32-C36 1551.72–1546.92 nm	89.85 ± 1.50	98.91 ± 0.47	87.05 ± 1.73	95.96 ± 0.96
C31-C37 1552.25–1547.72 nm	90.86 ± 1.76	98.34 ± 0.72	90.50 ± 1.70	97.07 ± 0.93
C30-C38 1553.33–1546.92 nm	80.87 ± 3.11	98.25 ± 0.93	82.79 ± 2.71	97.48 ± 1.03

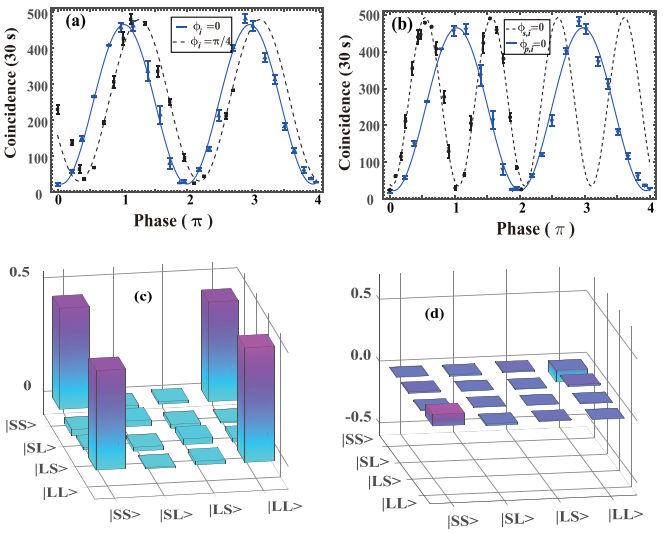

FIG. 3. Two-photon interference fringes and reconstructed density matrix for multiplexed time-bin-entangled photon pairs. (a) Coincidences in 30 s as a function of the signal UMI phase, when the pump UMI phase is fixed at 0 and the idler UMI phase is fixed at 0 (solid blue line) and $\pi/4$ (dashed black line). (b) Coincidences in 30 s when pump and idler UMI phases are fixed at 0 (solid blue line) and the signal and idler UMI phases are fixed at 0 (dashed black line). (c) and (d) Real and imaginary parts of our experimental reconstructed density matrix.

is prepared in state $|\Psi\rangle_p = 1/\sqrt{2}(|S\rangle - e^{i\phi_p}|L\rangle)$, where S and L signify the photon passing through the short and long arms of the interferometer, respectively, and ϕ_p is the relative phase between the two arms. After transmitting the pump beam from the DSF, time-bin entanglement is created from the two time slots with the states expressed as [15]

$$|\Phi\rangle = \frac{1}{\sqrt{2}}(|SS\rangle - e^{i2\phi_p}|LL\rangle). \quad (2)$$

When this entanglement state is further transformed by two UMIs in the signal and idler ports and we postselect the central slot, two-photon interference fringes are obtained. The coincidence for two photons is proportional to $1-V\cos(2\phi_p-\phi_s-\phi_i)$, where ϕ_s and ϕ_i are the relative phases of the UMIs in the signal and idler ports, respectively.

To characterize the quality of our time-bin-entangled source in detail, we measure the dependence of the two-photon interference with respected to the pump, signal, and idler UMI phases (ϕ_p, ϕ_s, and ϕ_i) by tuning the temperatures of the three UMIs. From the results shown in Figs. 3(a) and 3(b), the pump phase [Fig. 3(a)] is kept at 0 and the idler phase is kept at 0 and $\pi/4$ for the solid blue and dashed black curves, respectively. The raw (net) visibilities are 90.45 ± 2.30% (98.58 ± 0.85%) and 87.65 ± 2.59% (95.14 ± 1.62%). The two curves in Fig. 3(b) show the results for $\phi_p = \phi_i = 0$(solid blue line) and $\phi_s = \phi_i = 0$ (dashed black line) verifying that the two-photon interference fringe has a period of oscillation of π for the pump phase and 2π for the signal (idler) phase.

To fully characterize a quantum state, quantum state tomography is required. We use the method introduced in Ref. [38] to project measurements onto the different bases. The real and imaginary parts for our reconstructed density matrix are shown in Figs. 3(c) and 3(d), respectively. The raw (net) fidelity of our experimental density matrix from the ideal density matrix is 0.9120 ± 0.0120 (0.9723 ± 0.0070). A high fidelity for the reconstructed density matrix confirms the good quality of our time-bin-entangled source.

To demonstrate the feasibility of distributing our time-bin-entangled source over multiple channels, we measure the visibilities of the three correlated channel pairs. The results (Table II) show that the raw visibilities are above 84% and the net visibility is above 95%, implying that all channel pairs have high entanglement quality and are suitable for the all-fiber distribution of time-bin entanglement to multiple users using the DWDM technique.

To further characterize the properties of the sources, we perform the $g^{(2)}_{ss}$ autocorrelation and a heralded $g^{(2)}(0)$ measurement to show the purity and single-photon nature of the source. In the measurement, the pump power is 100 μW. We obtain an autocorrelation value of 1.761, which means that the purity of the source is 0.761 as $g^{(2)}_{ss} = 1 + P$, where P is the purity of the source [39]. The heralded $g^{(2)}(0)$ measurement yields a value of 0.0725, which means that the photon source has a good single-photon nature.

IV. DISCUSSION AND CONCLUSION

Polarization-entangled and time-bin-entangled photon sources are two of the more important quantum resources for quantum computation and quantum communications. In this study we prepared both kinds of entangled source based on SFWM in DSF at room temperature. The highest CAR was reached for the DSF-based photon-pair source operating at room temperature. We also verified the simultaneous presence of high entanglement over three channel pairs and the capability to use our source to distribute both kinds of entanglement to multiple users using the DWDM technique, performed with a DSF-based photon-pair source. Time-bin entanglement is much more suitable for long-distance transmission in optical fiber than polarization entanglement as it is not sensitive to po-

TABLE II. Visibilities for different channel pairs for a 100-μW pump and 30-s coincidences.

Channel pairs	Count (APD1, k/s)	Count (APD2, k/s)	Raw V (%)	Net V (%)
C32-C36 1551.72–1546.92 nm	6.4	20.0	87.35 ± 2.41	97.74 ± 0.99
C31-C37 1552.25–1547.72 nm	5.8	18.0	89.42 ± 2.35	96.85 ± 1.26
C30-C38 1553.33–1546.92 nm	5.0	19.0	83.98 ± 3.65	95.24 ± 1.99

larization distortion. For long-distance transmission of polarization in optical fiber one needs to actively stabilize the polarization fluctuation caused by temperature and stress variances.

Although relatively high performances are obtained for our source, further improvements of our DWDM entangled sources are feasible. In Ref. [27] the authors achieved entangled photon pairs over 40 channels, and entanglement in the whole *C* band is realized in Ref. [26]. In the present demonstration, the number of channel pairs was limited to three. By engineering the dispersion properties of the DSF or using high nonlinear fiber with shorter fiber length, the number of channel pairs can be greatly extended. The intense Raman scattering noise present in the DSF photon source under room-temperature operation limits any further increase in the CAR. By cooling the fiber to liquid-nitrogen (77 K) or helium (4 K) temperatures, noise from the photon signal can be greatly reduced. The APDs used in our experiments have a relative low efficiency, large time jitters, and long dead time. By using high-performance superconductor single-photon detectors, the coincidence count rate can be greatly enhanced and the CAR can be further improved by applying a narrower coincidence window.

Quantum information processing based on integrated optical elements such as optical fibers and silicon on insulator waveguide looks very promising for quantum networks. With advances in chip-scale quantum state engineering and telecom band fiber-based quantum memory, our all-fiber-based photon-pair entangled source is directly compatible with these systems in realizing the more complex tasks associated with computation and communication.

In conclusion, we prepared both polarization- and time-bin-entangled photon pairs based on a DSF operating at room temperature. By taking advantage of the state-of-art DWDM technique, our entanglement source looks promising in being able to perform an entanglement distribution over multiple users. The present work contributes to constructing an all-fiber-based long-distance quantum network that would provide a scalable, practical, and compact platform for quantum technology.

ACKNOWLEDGMENTS

We thank Dr. Shuang Wang for technical support in providing high-quality unbalanced Michelson interferometers. This work was supported by the National Fundamental Research Program of China (Grant No. 2011CBA00200), the National Natural Science Foundation of China (Grants No. 11174271, No. 61275115, No. 61435011, and No. 61525504), and the Fundamental Research Funds for the Central Universities.

Y.-H.L. and Z.-Y.Z. contributed equally to this work.

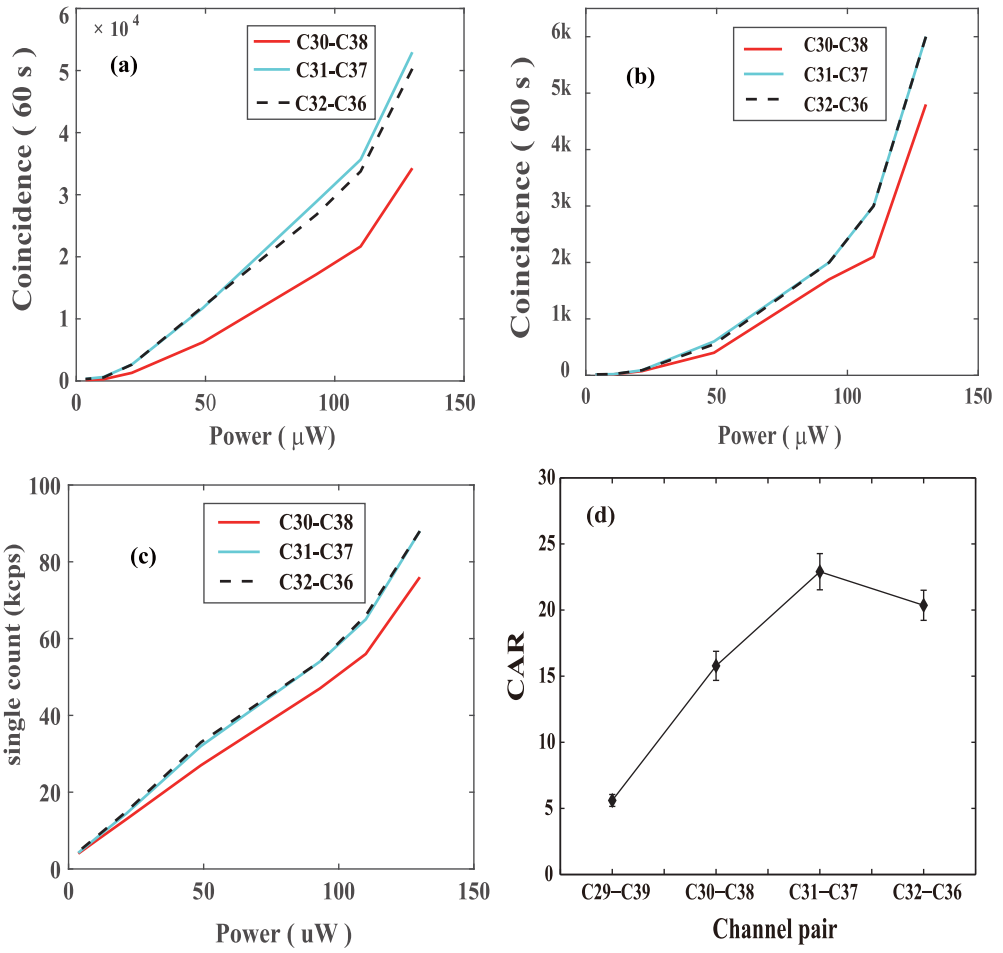

FIG. 4. (a) Coincidence count, (b) accidental coincidence count, and (c) single count for correlated channel pairs C30-C38 (bottom solid red line), C31-C37 (top solid light blue line), and C32-C36 (dotted black line). (d) CAR for four correlated channel pairs.

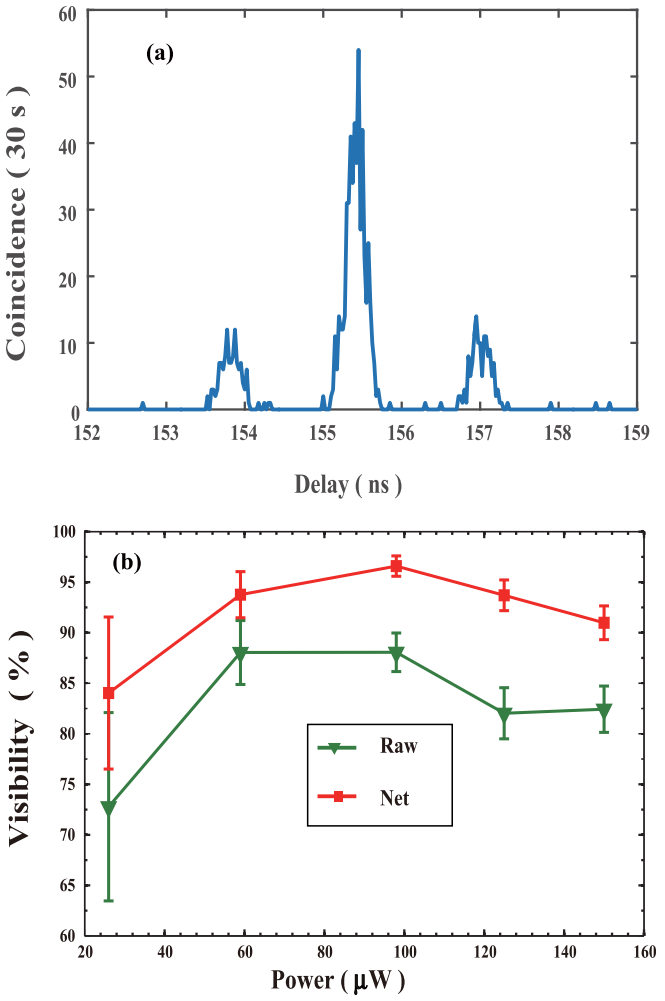

FIG. 5. (a) Histograms for 25-ps bin in time-bin-entanglement measurement. (b) Raw (bottom green line) and net (top red line) visiblities at different pump power.

APPENDIX

1. More data about the photon source

In the single-pass configuration, we measure the coincidence count, accidental coincidence count, and single count for three correlated channel pairs C30-C38 (bottom solid red line), C31-C37 (top solid light blue line), and C32-C36 (dotted black line). Results are showed in Figs. 4(a)–4(c). All the channel pairs have similar characteristics when the pump power is increasing. Channel pairs C31-C37 and C32-C36 are nearly the same because they are at the center of the emission spectra of the photon pairs; channel pair C30-C38 has a relatively lower count because it is near the boundary of the emission spectra. Figure 4(d) shows the CAR for four correlated channel pairs when the pump power is fixed at 41.4 uW. The CAR is decreasing with the frequency detuning from the central pump frequency. Because of the limited emission bandwidth of the photon source, the number of correlated channel pairs is small.

2. More data about the time-bin source

The histogram for a typical measurement is showed in Fig. 5(a): The bin width is 25 ps for each bin and the time difference of the peak is 1.6 ns. The performance of the time-bin source for channel pair C31-C37 at various pump powers is shown in Fig. 5(b). In the low-pump-power regime, the raw (bottom green line) and net (top red line) visibilities increase with increasing pump power, while in the high-pump-power regime, the visibility decreases with increasing pump power because of the multiphoton effect.

3. How the UMI phase is tuned in the time-bin source

The thermal coefficient of fiber at 1550 nm is $\frac{dn}{dT} = 0.811 \times 10^{-5}\,^{\circ}\mathrm{C}$, the fiber length difference of the UMI is 163.48 mm, and $L_d = c\Delta t/2n$ for a 1.6-ns delay. The temperature for one tuning period $\Delta T = \lambda/2L_d\frac{dn}{dT}$ is 0.585 K. In the experiments, the temperature tuning periods and the phase of the UMIs are measured and calibrated using a stable narrow bandwidth laser source. The phase of the UMIs can remain unchanged for hours because of serious thermal and acoustic isolation from the environment.

[1] D. Bouwmeester, J.-W. Pan, K. Mattle, M. Eibl, H. Weinfurter, and A. Zeilinger, Nature (London) **390**, 575 (1997).
[2] I. Marcikic, H. de Riedmatten, W. Tittel, H. Zbinden, and N. Gisin, Nature (London) **421**, 509 (2003).
[3] X.-L. Wang, X.-D. Cai, Z.-E. Su, M.-C. Chen, D. Wu, L. Li N.-L. Liu, C.-Y. Lu, and J.-W. Pan, Nature (London) **518**, 516 (2015).
[4] K. Mattle, H. Weinfurter, P. G. Kwiat, and A. Zeilinger, Phys. Rev. Lett. **76**, 4656 (1996).
[5] M. W. Mitchell, J. S. Lundeen, and A. M. Steinberg, Nature (London) **429**, 161 (2004).
[6] T. Nagata, R. Okamoto, J. L. O'Brien, K. Sasaki, and S. Takeuchi, Science **316**, 726 (2007).
[7] G. Brida, M. Genovese, and I. R. Berchera, Nat. Photon. **4**, 227 (2010).
[8] P. G. Kwiat, K. Mattle, H. Weinfurter, A. Zeilinger, A. V. Sergienko, and Y. Shih, Phys. Rev. Lett. **75**, 4337 (1995).
[9] Y. Li, Z.-Y. Zhou, D.-S. Ding, and B.-S. Shi, Opt. Express **23**, 28792 (2015).
[10] A. Martin, A. Issautier, H. Herrmann, W. Sohler, D. B. Ostrowsky, O. Alibart, and S. Tanzilli, New J. Phys. **12**, 103005 (2010).
[11] A. Kuzmich, W. P. Bowen, A. D. Boozer, A. Boca, C. W. Chou, L.-M. Duan, and H. K. Kimble, Nature (London) **423**, 731 (2003).
[12] D. S. Ding, Z. Y. Zhou, B. S. Shi, X. B. Zou, and G. C. Guo, Opt. Express **20**, 11433 (2012).

[13] X. Li, P. L. Voss, J. E. Sharping, and P. Kumar, Phys. Rev. Lett. **94**, 053601 (2005).
[14] H. Takesue and K. Inoue, Phys. Rev. A **70**, 031802 (2004).
[15] H. Takesue and K. Inoue, Phys. Rev. A **72**, 041804 (2005).
[16] S. X. Wang and G. S. Kanter, IEEE J. Sel. Top. Quantum Electron. **15**, 1733 (2009).
[17] J. W. Silverstone *et al.*, Nat. Photon. **8**, 104 (2014).
[18] C. Reimer *et al.*, Nat. Comunn. **6**, 8236 (2015).
[19] C. Reimer *et al.*, Science **351**, 1176 (2016).
[20] J. Fulconis, O. Alibart, J. L. O'Brien, W. J. Wadsworth, and J. G. Rarity, Phys. Rev. Lett. **99**, 120501 (2007).
[21] J.-W. Pan, Z.-B. Chen, C.-Y. Lu, H. Weinfurter, A. Zeilinger, and M. Zukowski, Rev. Mod. Phys. **84**, 777 (2012).
[22] H. J. Kimble, Nature (London) **453**, 1023 (2008).
[23] H. C. Lim, A. Yoshizawa, H. Tsuchida, and K. Kikuchi, Opt. Fiber Tech. **16**, 225 (2010).
[24] Z.-Y. Zhou, Y.-K. Jiang, D.-S. Ding, B.-S. Shi, and G.-C. Guo, Phys. Rev. A **87**, 045806 (2013).
[25] I. Herbauts, B. Blauensteiner, A. Poppe, T. Jennewein, and H. Hubel, Opt. Express **21**, 29013 (2013).
[26] D. Aktas, B. Fedrici, F. Kaiser, T. Lunghi, L. Labonte, and S. Tanzilli, Laser Photon. Rev. **10**, 451 (2016).
[27] H. C. Lim, A. Yoshizawa, H. Tsuchida, and K. Kikuchi, Opt. Express **16**, 22099 (2008).
[28] F. Kaiser, D. Aktas, B. Fedrici, T. Lunghi, L. Labonte, and S. Tanzilli, Appl. Phys. Lett. **108**, 231108 (2016).
[29] C. Autebert, J. Trapateau, A. Orieux, A. Lemaître, C. Gomez-Carbonell, E. Diamanti, I. Zaquine, and S. Ducci, arXiv:1607.01693.
[30] K. F. Lee, J. Chen, C. Liang, X. Li, P. L. Voss, and P. Kumar, Opt. Lett. **31**, 1905 (2006).
[31] S. Dong, Q. Zhou, W. Zhang, Y. He, W. Zhang, L. You, Y. Huang, and J. Peng, Opt. Express **22**, 359 (2014).
[32] J. Jin, E. Saglamyurek, M. l. G. Puigibert, V. Verma, F. Marsili, S. W. Nam, D. Oblak, and W. Tittel, Phys. Rev. Lett. **115**, 140501 (2015).
[33] E. Saglamyurek, J. Jin, V. B. Verma, M. D. Shaw, F. Marsili, S. W. Nam, D. Oblak, and W. Tittel, Nat. Photon. **9**, 83 (2015).
[34] E. Saglamyurek *et al.*, Nat. Comunn. **7**, 11202 (2015).
[35] J. F. Clauser, M. A. Horne, A. Shimony, and R. A. Holt, Phys. Rev. Lett. **23**, 880 (1969).
[36] S. Wang, W. Chen, J.-F. Guo, Z.-Q. Yin, H.W. Li, Z. Zhou, G.-C. Guo, and Z.-F. Han, Opt. Lett. **37**, 1008 (2012).
[37] S. Wang, Z.-Q. Yin, W. Chen, D.-Y. He, X.-T. Song, H.-W. Li, L.-J. Zhang, Z. Zhou, G.-C. Guo, and Z.-F. Han, Nat. Photon. **9**, 832 (2015).
[38] H. Takesue and Y. Noguchi, Opt. Express **17**, 10976 (2009).
[39] N. Bruno, A. Martin, T. Guerreiro, B. Sanguinetti, and R. T. Thew, Opt. Express **22**, 17246 (2014).